

Solar-driven absorption cooling system with latent heat storage for extremely hot climates

Sajid Mehmood^{a,b,*}, Jesus Lizana^{c,d}, Daniel Friedrich^a

^a School of Engineering, Institute for Energy Systems, The University of Edinburgh, Colin Maclaurin Road, Edinburgh EH9 3DW, United Kingdom

^b Department of Mechanical, Mechatronics and Manufacturing Engineering (New Campus), University of Engineering & Technology, Lahore, Pakistan

^c Department of Engineering Science, University of Oxford, Parks Road, Oxford OX1 3PJ, United Kingdom

^d Future of Cooling Programme, Oxford Martin School, University of Oxford, Oxford OX1 3BD, United Kingdom

ARTICLE INFO

Keywords:

Solar-driven absorption cooling
Phase change materials
Renewable cooling
Evacuated tube collector
Life cycle cost

ABSTRACT

Novel renewable cooling systems are required worldwide to address the growing demand for cooling. This study proposes and demonstrates a novel integration of solar-driven absorption cooling with latent heat storage to maximise the use of renewable energy for cooling in extremely hot climates. A parametric analysis was performed in TRNSYS to identify the critical parameters for optimal sizing related to the solar field size, tank volume, tank insulation, auxiliary heating set point, and collector tilt angle. Moreover, the integration was compared with a conventional solar-driven absorption cooling system using sensible heat storage (a hot water tank) and an electric-driven vapour compression cooling system. The results show that a solar field size of 1.5 m²/kW_c, a latent heat storage tank volume of 30 L/m², adequate insulation below 0.8 W/m².K, and appropriate set-point temperatures for the auxiliary boiler provide the optimal performance to maximise the solar fraction. Compared with conventional solar-driven absorption cooling, the study demonstrates how the phase change material (PCM) increased the solar fraction by 4.2 % (from 70.3 to 74.5 %) due to higher stable temperature and lower tank losses (reduced by 44 %). In addition, despite the higher initial investment cost of the proposed PCM-based solar-driven cooling system compared to the vapour compression cooling system, the findings highlight that the life cycle cost is much lower in extremely hot climates. After 25 years, the life cycle cost was lowered by 34 % compared to vapour compression and by 9 % compared to a conventional solar-driven cooling system. Compared to vapour compression refrigerant technology, the proposed system can save 31.6 % of primary energy and 1222 kgCO_{2eq} annually. This research provides valuable insights into the optimal design and integration of renewable cooling for residential applications in extremely hot regions.

1. Introduction

The energy demand for space cooling is increasing globally [1]. The expected increase in cooling demand by 2050 is equivalent to more than 20 % of total global electricity consumption in 2016 [2]. This growing demand is specifically sharp in extremely hot regions, adding pressure on local grids and generating a significant challenge [3]. This challenge is even more pronounced in developing countries where electricity from imported fossil fuels strains national finances [4].

Currently, the dominant cooling technology in the market for space cooling is based on vapour compression systems (VCS), which are energy-intensive and use pollutant refrigerants. In the event of a leak, these refrigerants can significantly contribute to global warming in the

short term, with a global warming potential up to 14,800 times greater than carbon dioxide [5,6]. There is an urgent need for clean, affordable cooling technologies that can reduce peak load demand for electricity, lower reliance on fossil fuels, increase resilience, and reduce greenhouse gas emissions [7].

One promising alternative to conventional VCS is solar-driven absorption cooling systems (ACS) for cooling applications [8–10]. Typically, the highest cooling requirements arise during the daytime when solar radiation is at its highest intensity. This synchronisation presents a remarkable advantage in utilising solar energy for cooling needs. ACS offers an eco-friendly and sustainable substitute for conventional cooling systems, mitigating dependence on fossil fuels and associated emissions. However, the design and implementation of these systems present different challenges. The high investment cost, intermittent heat

* Corresponding author at: Department of Mechanical, Mechatronics and Manufacturing Engineering (New Campus), University of Engineering & Technology, Lahore, Pakistan.

E-mail address: s.mehmood@ed.ac.uk (S. Mehmood).

<https://doi.org/10.1016/j.enconman.2023.117737>

Received 8 July 2023; Received in revised form 9 September 2023; Accepted 3 October 2023

Available online 10 October 2023

0196-8904/© 2023 The Authors. Published by Elsevier Ltd. This is an open access article under the CC BY license (<http://creativecommons.org/licenses/by/4.0/>).

Nomenclature			
a_0	optical efficiency of collector	G	solar irradiance
a_1	first-order heat loss coefficient	HW	hot water
a_2	second-order heat loss coefficient	LCC	life cycle cost
ACS	absorption cooling system	LHS	latent heat storage
A_a	collector aperture area	NMBE	normalised mean bias error
A_{top}	area of the top surface of the tank	PCM	phase change material
C_a	acquisition cost (initial purchase cost)	PEC _{ACS}	primary energy consumption of absorption cooling system
CDE	total annual carbon dioxide equivalent emissions	PEC _{VCS}	primary energy consumption of vapour compression system
CDE _e	emissions produced from the electricity	PEF _e	primary energy factor for electricity
CDE _{ng}	emissions produced from the natural gas in the auxiliary boiler	PEF _{ng}	primary energy factor for natural gas
c_e	unit cost of electricity	Q _{aux}	amount of energy from the auxiliary source
CHW	chilled water	Q _{loss,cond}	energy losses from collector due to conduction
C_m	maintenance costs	Q _{loss,conv}	energy losses from collector due to convection
c_{ng}	unit cost of natural gas	Q _{loss,opt}	energy losses due to the optical properties of the collector
C_o	operating costs	Q _{loss,rad}	energy losses from collector due to radiation
C_p	specific heat capacity of fluid	Q _{loss,top}	amount of energy lost from the top surface of the tank
CV-RMSE	coefficient of variation of root mean square error	Q _{losses}	energy losses from the collector
CW	cooling water	Q _{solar}	amount of energy from the solar
E _e	annual electricity consumption	Q _u	useful energy gain from the collector
EES	engineering equation solver	Q _i ^{hx}	heat transfer with the immersed heat exchanger
EF _{co2,e}	carbon dioxide equivalent emissions factor for electricity	Q _i ^{aux}	heat supply from an auxiliary heater
EF _{co2,ng}	carbon dioxide equivalent emissions factor for natural gas	Q _i ^{cod}	heat conduction towards adjacent nodes of storage tank
E _{ng}	annual natural gas consumption	Q _i ^{loss}	heat dissipation to the surroundings
ETC	evacuated tube collector	R ²	coefficient of determination
FC _e	annual cost of electricity	SF	solar fraction
FC _{ng}	annual cost of natural gas	SHS	sensible heat storage
FPC	flat plate collector	TES	thermal energy storage
		VCS	vapour compression system

from the sun, and limited rooftop space are some examples of its limitations for effective implementation at a residential scale [8].

Khan et al. [11] examined the performance of ACS for cooling an educational facility using the TRNSYS software. They employed a flat plate collector (FPC) and an evacuated tube collector (ETC) in two configurations. The first configuration had the hot water outlet temperature flowing back to the storage tank, while the second configuration used a control strategy to direct the fluid toward the tank only if it was lower than the tank's average temperature. If the temperature was higher, it bypassed the tank and went toward the auxiliary boiler loop. The study showed that the ETC and the second configuration were the most effective. Angrisani et al. [12] modelled ACS with TRNSYS with one concentrating (parabolic collector) and two non-concentrating collectors in Iraq. They found that concentrating collectors perform better than non-concentrating collectors for the investigated climate. Bellos et al. [13] developed an ACS model to analyse its performance with different collectors in Greece using the Engineering Equation Solver (EES). An optimisation was carried out for each system to determine the minimum collecting area required. The ETC was deemed the most suitable option based on financial criteria. The economic benefits of ETC over FPC were also shown by Tashtoush et al. [14]. Other studies focused on investigating the performance of ACS with different refrigerant pairs to enhance its performance [10,15–17]. More common working pairs found in this context are LiCl-H₂O, LiBr-H₂O and NH₃-H₂O.

Shirazi et al. [18] created a simulation model of an ACS to analyse its performance while utilising fixed and variable speed pumps and implementing various control strategies for the collector loop. Additionally, they assessed the effectiveness of two configurations for an auxiliary boiler, one in series and another in parallel. The study demonstrated the advantages of employing a variable speed pump in the collector loop and utilising an auxiliary boiler in a parallel rather than a

series configuration. Atmaca et al. [19] investigated the ACS performance in Antalya (Turkey). They analysed the impact of collector and storage tank parameters. They discovered that an oversized storage tank could negatively affect the system's performance. Al-Alili et al. [20] created a computational model for a 10 kW ACS that employed an NH₃-H₂O refrigerant pair and an evacuated tube collector in Abu Dhabi. Their study emphasised the critical importance of selecting appropriately sized components to reduce the payback period, such as the solar field size or TES. They found that carefully selecting these components can significantly impact the system's performance and financial viability. Altun et al. [21] studied the feasibility of using an ACS with an optimal configuration in six distinct Turkish climates, focusing on the control strategy for the auxiliary boiler. The results showed that an appropriate control strategy can lead to significant cost savings, improved energy efficiency, and a payback period of around ten years in areas with high cooling demand. Buonomo et al. [22] analysed the ACS performance with a numerical model developed in TRNSYS using three different fluids in a collector loop: pure water, Al₂O₃-water nanofluids with 3 % concentration, and Al₂O₃-water nanofluids with 6 % concentration. Their results demonstrated that using Al₂O₃-water nanofluids with a 6 % concentration could lead to up to 6 % primary energy savings. Habib et al. [23] explored integrating a solar-driven ACS with a desiccant-based air conditioning system to separately address sensible and latent loads. They found that radiant cooling, using chilled water from an absorption chiller, primarily managed the sensible cooling load, while a solid desiccant dehumidification system effectively handled the latent load. Simulation results using TRNSYS indicated that this integrated approach could achieve a higher thermal coefficient of performance (COP) than a standalone absorption cycle. Nienborg et al. [24] developed various control strategies in TRNSYS to optimise the operation of ACS with minimum energy consumption of fans and pumps. The researchers showed that using smart control strategies and variable-speed

fans and pumps could lead to up to 25 % electricity savings compared to conventional fixed-speed fans and pumps.

The literature indicates that researchers have primarily focused on analysing the performance of ACS using different types of collectors, various fluids in collector loops, different refrigerant pairs, configurations, and control strategies. However, no previous studies have considered the potential of phase change materials (PCM) to improve ACS performance (*research gap 1*) [25,26]. Moreover, only a few studies have analysed the performance of solar-driven ACS in extremely hot regions, where higher synergies between cooling needs and solar availability are found (*research gap 2*) [27,28]. All previous studies have exclusively considered sensible heat storage (SHS) systems, such as water tanks, mainly in temperate climate zones, leaving an important gap in the benefits of latent heat storage (LHS) to increase the solar fraction of ACS located in extremely hot regions. SHS involves storing heat by increasing the medium temperature. In contrast, LHS involves storing heat when a material undergoes a phase change, for example, from solid to liquid. Compared to SHS, LHS through PCM can provide stable output temperatures at a higher TES density, reducing heat losses, maximising system capacity, and increasing renewable usage [29–32].

This research analyses the benefits of LHS to increase the use of renewable energy for solar-driven absorption cooling in extremely hot climates. The novelty lies in an advanced integration of PCM for solar-driven cooling designed explicitly for the environmental conditions of extremely hot regions. The system has been optimised through a parametric analysis in TRNSYS considering solar field size, storage tank size, auxiliary boiler set-point temperature, and tilt angle of the collector. A typical residential archetype in the extremely hot climate of Sukkur (Pakistan) was used as a reference case for the residential cooling demand profile. The results compare the energy, environmental and economic performance of this novel integration with a conventional solar-driven ACS based on sensible heat storage (using a hot water tank), and an electric-driven VCS. Two research contributions are provided in this study to support renewable cooling:

- The benefit of latent heat storage to increase the fraction of solar renewable energy for solar-driven absorption cooling was demonstrated through an advanced numerical model (*addressing research gap 1*).
- The energy, environmental and economic performance of PCM-based solar-driven absorption cooling for extremely hot regions in Southern Asia were quantified, providing valuable insights into the challenges and opportunities for renewable cooling in these climates (*addressing research gap 2*).

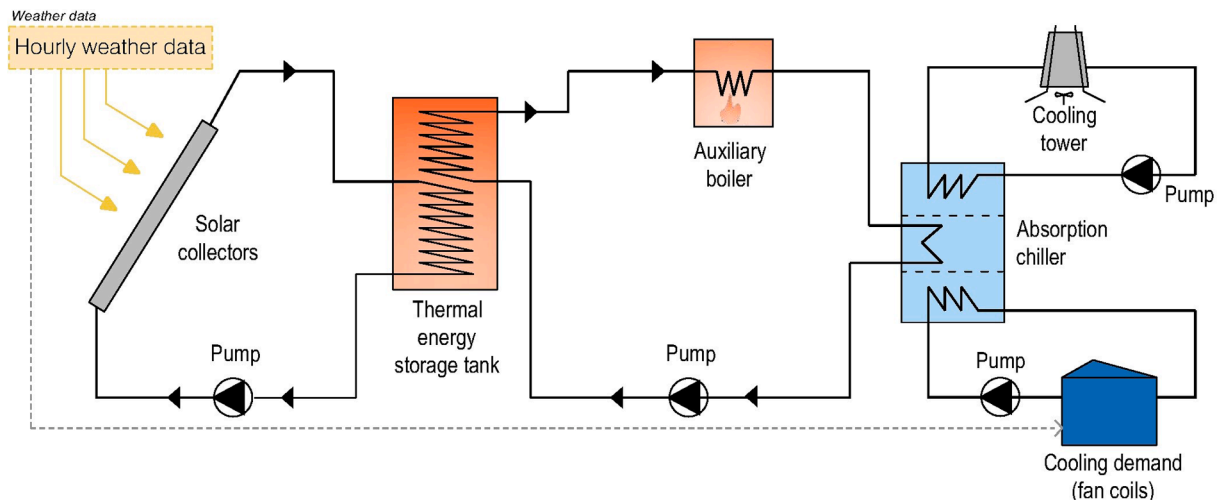


Fig. 1. Schematic diagram of the proposed PCM-based solar-driven absorption cooling.

This paper is structured as follows. Section 2 briefly introduces the PCM-based solar-driven ACS configuration and describes the main components. Section 3 is divided into two sub-sections. Section 3.1 defines all data related to the selected climate and the reference case study. Section 3.2 details the methods employed for the numerical modelling. Results are shown in Section 4, with different sub-sections covering the cooling demand profile, the parametric analysis for optimal sizing, the performance of the solar-driven cooling system with and without PCM, the comparison with vapour compression refrigerant technology, and the life cycle cost (LCC) analysis. Finally, conclusions were drawn in Section 5.

2. System description

The global schematic diagram of the proposed solar-driven absorption cooling with latent heat storage is illustrated in Fig. 1. It integrates seven main components: solar collector, thermal energy storage based on PCM, auxiliary boiler, pumps, cooling tower, absorption chiller, and fan coil units.

Solar collectors consist of evacuated tube collectors (ETC), able to achieve higher efficiencies than FPC due to the high operating temperature range (from 70 °C to 120 °C).

TES tank integrates two inner coils immersed in the PCM. The selected PCM has the potential to store up to 150 kJ/kg of energy within the temperature range between 88 and 90 °C.

The auxiliary boiler provides additional energy to operate the absorption chiller on cloudy days or when there is not enough solar radiation to drive the absorption chiller.

The absorption chiller is energised by the thermal energy derived from hot water. The selected absorption chiller has a cooling capacity of 17.6 kW. It uses a lithium bromide (LiBr) and water (H₂O) as its operational substances, where water functions as the refrigerant and lithium bromide, a nontoxic salt, as the absorbent.

Pumps selected for this system consist of variable speed pumps capable of maintaining the mass flow rate within a range from zero to its rated value. The pump's mass flow rate adjusts in response to changes in the control signal settings.

The cooling tower chosen for this system is a counterflow forced-draft cooling tower, wherein hot water interacts directly with an air stream, leading to cooling through both sensible heat transfer due to temperature difference with the air and mass transfer brought about by evaporation.

Cooling demand was defined according to a residential building archetype model in Pakistan, previously used and validated in [3,33]. The selected house is representative of the building stock of Pakistan.

This integration was assessed in the climatic conditions of Sukkur (Pakistan). According to the ASHRAE 169 climate zone classification, this region falls under an extremely hot climate [3]. The outdoor hourly air temperature varies from 5.5 to 50 °C in the Sukkur area.

3. Materials and methods

This section is divided into two sub-sections. Section 3.1 defines the weather data of the selected location and building archetype used in the model. Section 3.2 details the methods used for the numerical energy modelling in TRNSYS and the parametric analysis.

3.1. Materials

3.1.1. Climate

This study uses recent typical meteorological weather files collected from “Climate.OneBuilding.Org” [34], an online repository of free climatic data for energy modelling. Fig. 2(a) and (b) display the hourly variations of dry bulb temperature and monthly solar irradiance on a horizontal surface.

An extremely hot temperature zone characterises the climate in

Sukkur [3], with the summer season lasting from April to October and peak temperatures occurring in May, June, and July. Hourly outdoor air temperatures range from 5.5 to 50 °C, with more than 15 % of the year exceeding 38 °C. The monthly mean temperature ranges from 33 to 37 °C in summer to 15–22 °C in winter.

Regarding solar irradiance, Sukkur (Pakistan) experiences high solar irradiance levels. The yearly daily average solar irradiance in Sukkur is 5.9 kWh/m², making this location a good option for solar-driven cooling technologies. The highest levels of global irradiance are in May, with a daily average value of 7.57 kWh/m² and a total of 234.7 kWh/m² per month. Conversely, December experiences the lowest solar radiation levels, with an average daily value of 3.8 kWh/m² and 118.2 kWh/m² per month.

3.1.2. Reference case study

This paper selected a typical two-story residential building as a case study. The building model was experimentally validated in a previous study where the performance of different passive cooling solutions was analysed [3]. The building archetype is a two-storey with a flat roof and a rectangular layout. Each floor comprises two bedrooms with attached bathrooms, a living room, a drawing room, and a kitchen. The house's

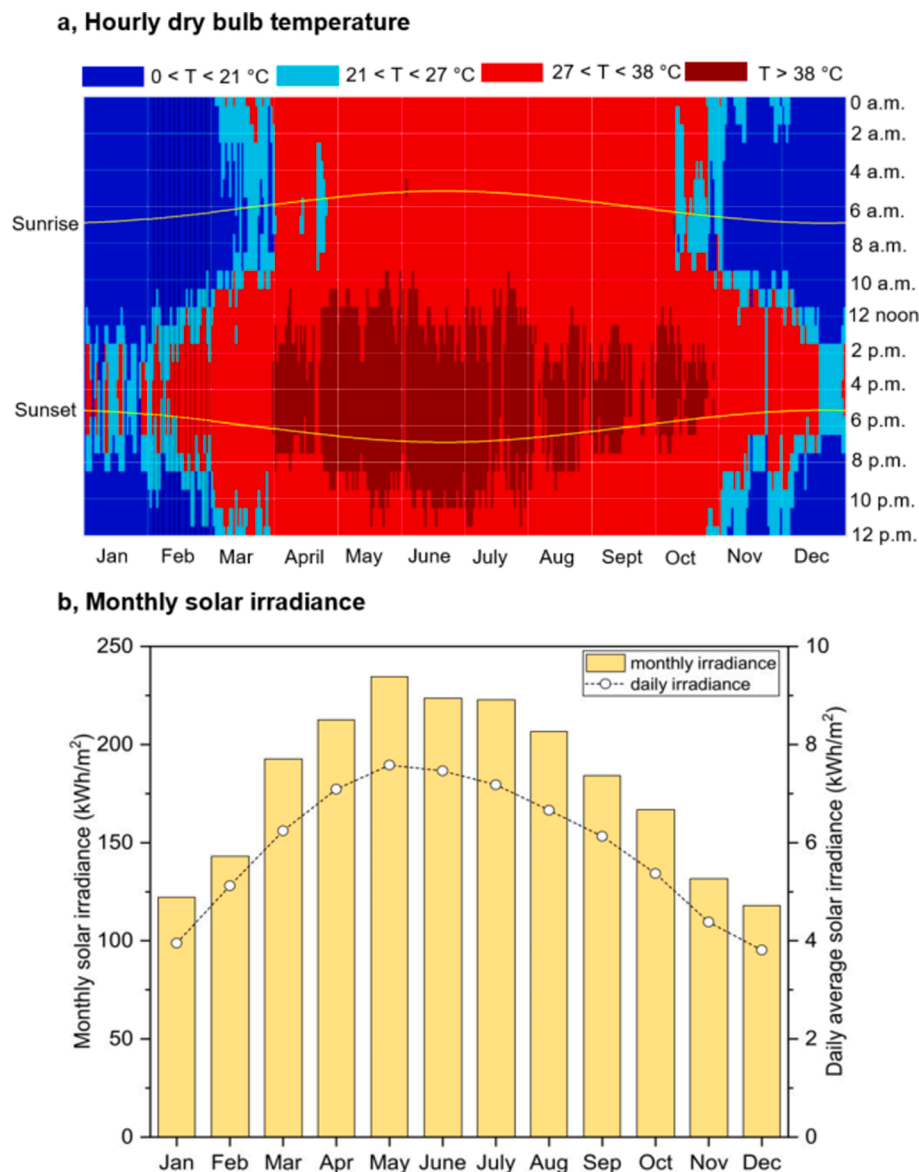


Fig. 2. Visualisation of weather data. a, Hourly dry bulb temperature. b, Monthly solar irradiance on a horizontal surface.

walls are made from clay bricks with cement mortar applied on both sides, while the roof is constructed using reinforced concrete with a mortar layer, bitumen, mud Phuska, and roof tiles. Occupant gains were calculated considering both no. of occupants and their activity levels. Occupancy profiles were considered as follows: two occupants in each bedroom from 10 pm to 7 am, two people in the living room from noon to 4 pm, and four people from 4 pm to 10 pm were assumed. The equipment and lighting heat gains were 3 W/m^2 and 2 W/m^2 , respectively, while thermal bridges were considered at $0.1 \text{ W/m}^2\text{K}$ of envelope area [35]. Infiltration leakage was defined by an ACH value of 1.2 h^{-1} , according to the procedure reported in Annex B of EN 15242:2007 [36]. Wall and façade solar absorptance values are 0.5 and 0.65, respectively. A geometric plan and further details of the selected building can be found in [3]. The hourly thermal cooling demand was calculated using design conditions fixed at 24°C in the daytime and 25°C at night.

3.2. Methods for numerical simulation

This section details the methods used for the numerical modelling and parametric analysis of the building, systems, and operating conditions.

3.2.1. Global numerical modelling and parametric study

The energy system simulation programme TRNSYS v18 was used for the numerical simulation and parametric analysis. TRNSYS is a highly flexible, graphical simulation platform for simulating the behaviour of transient systems.

First, a 3D building model with different thermal zones was created in Sketch Up. This model was subsequently imported into TRNSYS TRNBuild v3.0, where various properties of the building elements (including walls, windows, roof), internal gains (such as lighting, appliances, occupants), ventilation, infiltration, and their schedules were defined in detail. Once all properties were described, a “*.b18” file was generated with TRNBuild, which was input in Type 56 (multi-zone

building model) within the TRNSYS simulation studio to calculate the cooling demand of the residential building. Second, the PCM-based solar-driven ACS integration was characterised in the TRNSYS simulation studio to meet the hourly cooling demand generated by the building model. Third, a parametric study was conducted by writing a Python script to determine the optimal integration. The Python script runs the TRNSYS simulation, modifies the model’s input data in the TRNSYS deck file, and compiles the results.

The scheme of the simulation workflow for the parametric analysis is shown in Fig. 3. This workflow was repeated to compare the proposed PCM-based solar-driven ACS integration with a conventional ACS based on sensible heat storage (using a hot water tank), and an electric-driven VCS.

The process flowsheet of the PCM-based solar-driven ACS integration modelled in the TRNSYS simulation studio is illustrated in Fig. 4.

The major components used in TRNSYS for the different numerical models are shown in Table 1. The following sections further detail these numerical models and components used.

3.2.2. Numerical model of solar absorption cooling system

The following section details the solar-driven ACS model with two TES and different components (TRNSYS Types). The solar-driven ACS consists of four water loops, i.e., solar collector loop, hot water (HW) loop, cooling water (CW) loop, and chilled water (CHW) loop (see Fig. 4).

The first loop of solar-driven ACS is the collector loop. Solar energy is captured and converted to heat in the solar collector loop. Water is passed through the evacuated tube collectors and gets heated. A variable speed pump was used in the solar collector loop, and a feedback controller was used to adjust the fluid flow rate to control the outlet temperature of the collector. The collector performs better by regulating the flow rate in the solar collector loop by maintaining a fixed temperature difference between the inlet and outlet of the collector. This fixed temperature difference was controlled in the model using Type 2b (differential controller) and Type 22 (iterative feedback controller).

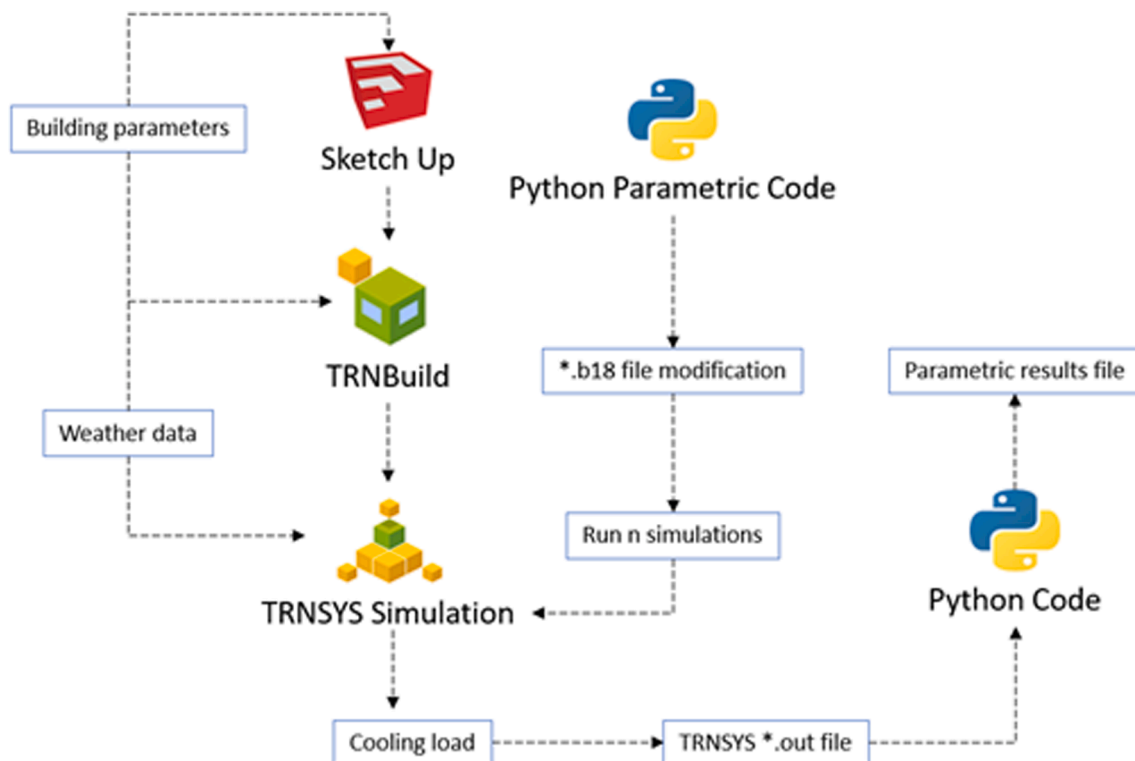


Fig. 3. Scheme of the simulation workflow for the parametric analysis.

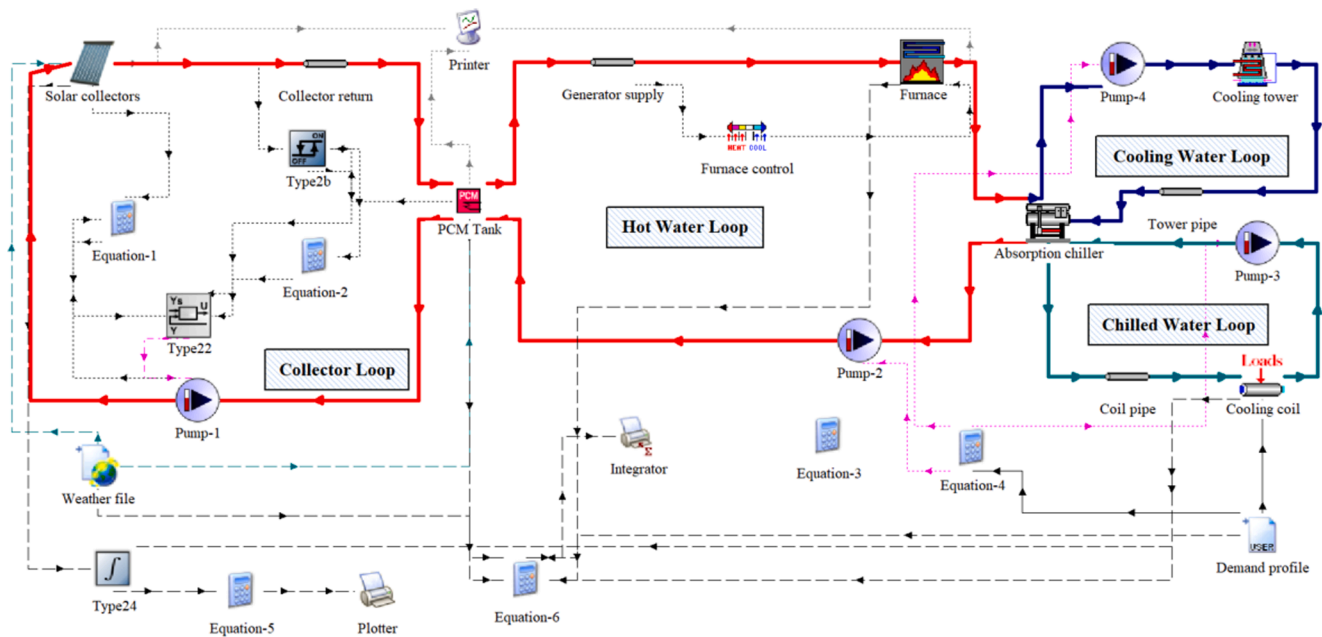


Fig. 4. Process flowsheet of the numerical simulation model developed in TRNSYS v18.

Table 1
TRNSYS types used to model the cooling systems.

Sr. no	TRNSYS Types	Function	PCM-based ACS	Conventional ACS	VCS
1	Type 71	Evacuated tube collector	x	x	
2	Type 110	Variable speed pump	x	x	
3	Type 2b	Differential controller	x	x	
4	Type 108	Five stage thermostat	x	x	x
5	Type 22	Iterative feedback controller	x	x	
6	Type 1571	PCM tank	x		
7	Type 156	Hot water tank		x	
8	Type 700	Auxiliary boiler	x	x	
9	Type 107	Absorption chiller	x	x	
10	Type 119	Air source heat pump			x
11	Type 31	Pipe	x	x	
12	Type 682	Cooling load imposed on a fluid stream	x	x	
13	Type 162	Cooling tower	x	x	
14	Type 15-3	Weather processor	x	x	x
15	Type 56	Multi-zone building model			x
16	Type 9c	Data reader	x	x	x
17	Type 24	Integrator	x	x	x
18	Type 25	Printer	x	x	x
19	Type 65	Plotter	x	x	x

Type 2b compares the upper (T_H) and lower input temperature (T_L) difference with the upper (ΔT_H) and lower dead band (ΔT_L) and provides an on ($\mu = 1$) or off signal ($\mu = 0$).

Mathematically, the control function can be written as follows:

If the controller was previously on ($\mu = 1$):

$$\text{if } \Delta T_L \leq (T_H - T_L) \text{ then } \mu = 1 \quad (1)$$

$$\text{if } \Delta T_L > (T_H - T_L) \text{ then } \mu = 0 \quad (2)$$

If the controller was previously off ($\mu = 0$):

$$\text{if } \Delta T_H \leq (T_H - T_L) \text{ then } \mu = 1 \quad (3)$$

$$\text{if } \Delta T_H > (T_H - T_L) \text{ then } \mu = 0 \quad (4)$$

The control function graphically can be shown in Fig. 5.

In this model, the collector outlet temperature was selected as the upper input temperature, tank temperature as the lower input temperature, an upper dead band of 10°C , and a lower dead band of 2°C . Following the logic provided in Eqs. (1) to (4), the controller generates a signal of on and off.

The TRNSYS Type 2b signal is fed to TRNSYS Type 22. The Type 22 in TRNSYS is an iterative feedback controller that maintains the controlled variable at the set point. In this model, the collector inlet and outlet temperature difference was set to 10°C with this controller by varying the pump's flow rate for higher collector efficiencies. This hot water from the solar collectors is then stored in the PCM tank (Fig. 4). The second loop is the hot water loop, where the hot water is used to operate the absorption chiller. In this loop, an auxiliary gas boiler is installed to increase the temperature if the tank temperature is insufficient. The third is the cooling water loop, where the condenser heat is

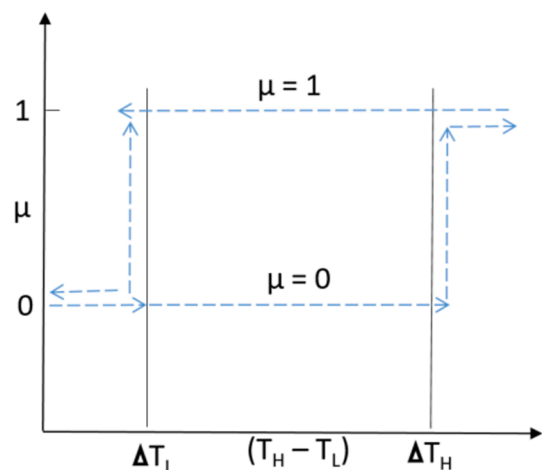


Fig. 5. Controller function.

dissipated via a cooling tower. The fourth loop is the chilled water loop, where the chilled water produced from the chiller fulfils the hourly cooling load requirements of the building. The operation of the absorption chiller was defined based on this hourly cooling demand profile. Whenever there is a need for cooling according to the occupant's schedules, as described in subsection 3.1.2, it turns on the absorption chiller and pumps in all associated loops for smooth operation.

The following subsections detail the mathematical modelling of different components used for this study.

3.2.2.1. Evacuated tube collector. This study uses TRNSYS Type 71 to simulate an evacuated tube collector. Equation (5) shows the energy balance of this collector at a steady state.

$$A_a G = Q_u + Q_{\text{losses}} \quad (5)$$

A_a represents the collector aperture area, G solar irradiance, and Q_u useful energy gain from the collector. Energy losses from the collector (Q_{losses}) are due to the optical properties of the collector absorber surface ($Q_{\text{loss, opt}}$) and by conduction ($Q_{\text{loss, conv}}$), convection ($Q_{\text{loss, cond}}$) and radiation ($Q_{\text{loss, rad}}$) from the collector surface, as written in equation (6).

$$Q_{\text{losses}} = Q_{\text{loss, opt}} + Q_{\text{loss, conv}} + Q_{\text{loss, cond}} + Q_{\text{loss, rad}} \quad (6)$$

The rate of useful energy gain (Q_u) and efficiency of the solar collector (η_{th}) can be expressed by equations (7) and (8), respectively [37].

$$Q_u = m C_p (T_{\text{out}} - T_{\text{in}}) \quad (7)$$

where m and C_p represent the water mass flow rate and specific fluid heat capacity, respectively. T_{out} and T_{in} represent the outlet and inlet temperatures of the collector.

$$\eta_{th} = a_0 - a_1 \left(\frac{T_m - T_{\text{amb}}}{G} \right) - a_2 \frac{(T_m - T_{\text{amb}})^2}{G} \quad (8)$$

where a_0, a_1, a_2 represent optical collector efficiency, and first and second-order heat loss coefficients, respectively. T_m shows the mean temperature from the collector, and T_{amb} shows the ambient temperature. The ETC characteristics for the simulation are defined in Table 2, according to the commercial solar collector Viessmann Vitosol 200 T SPE.

3.2.2.2. Thermal energy storage tanks. The performance of the ACS is evaluated through two TES scenarios, with the main characteristics of each detailed in Table 3.

The ACS was first integrated and optimised with latent heat storage based on a PCM tank using Rubitherm SP90, a commercially available PCM with a melting temperature of 90 °C. In addition, this integration was compared with a conventional ACS, which was simulated and optimised using sensible heat storage based on a hot water tank.

More details of the PCM and hot water tanks are provided below.

PCM storage tank: A new TRNSYS component was written and compiled in FORTRAN to model the PCM tank. This component's structure is based on the numerical model of Type 156, based on a stratified fluid tank for sensible storage within the TRNSYS platform. Using this reference model, the two flow streams that pass into and out

Table 2
Characteristics of solar collector for the model.

Parameters model	Units	Evacuated tube collectors
Collector area	m ²	Variable
Optical efficiency (a_0)	–	0.72
First-order heat loss coefficient (a_1)	W/m ² .K	1.21
Second-order heat loss coefficient (a_2)	W/m ² .K ²	0.0025
Weight (when empty)	kg	39
Collector slope	degree	variable
Collector azimuth	degree	0

Table 3

Characteristics of two TES alternatives considered for ACS.

Parameter	PCM Tank	Water Tank
Storage tank-specific volume (L/m ²)	30	75
Height of Tank (m)	2.31	3.13
Diameter of Tank (m)	0.66	0.89
Loss coefficient (W/m ² .K)	0.83	0.83

of the storage tank were eliminated, and sensible storage capacity was numerically changed into latent heat storage using the enthalpy approach, following the criteria defined by Lizana et al. [29,38]. This mathematical procedure of the enthalpy approach consists of a continuous and invertible function of the temperature. It means that for a given volume and material, a continuous and reversible function can be calculated, which will return the temperature (T) depending on the calculated enthalpy (h) [39,40]. The final model consists of a cylindrical vertical-oriented storage tank with a constant volume design equipped with an immersed heat exchanger. The PCM within the storage tank engages with the fluid in the heat exchanger, transferring heat through the immersed heat exchanger. It also interacts with the surroundings, losing heat from its upper, lower, and side sections. As a result, the energy balance (Q_i) of the PCM tank can be written as follows.

$$Q_i = Q_i^{hx} + Q_i^{aux} + Q_i^{cond} + Q_i^{loss} \quad (9)$$

Where (hx) represents the heat transfer with the immersed heat exchanger, while (aux) signifies the additional heat supply from an auxiliary heater. ($cond$) denotes the heat conduction towards adjacent nodes of a storage tank, and ($loss$) accounts for the dissipation to the surroundings (through thermal losses from the top, bottom, and sides according to Equations (10), (11), and (12).

$$Q_{\text{loss, top}} = A_{\text{top}} U_{\text{top}} (T_{\text{tank}} - T_{\text{env, top}}) \quad (10)$$

where $Q_{\text{loss, top}}$ shows the amount of energy lost from the top surface of the tank, A_{top} is the area of the top surface of the tank, U_{top} is the heat transfer coefficient from the top surface, T_{tank} is tank temperature and $T_{\text{env, top}}$ is surrounding or environmental temperature at the top surface of the tank.

$$Q_{\text{loss, bottom}} = A_{\text{bottom}} U_{\text{bottom}} (T_{\text{tank}} - T_{\text{env, bottom}}) \quad (11)$$

where $Q_{\text{loss, bottom}}$ shows the amount of energy lost from the bottom surface of the tank, A_{bottom} is the area of the bottom surface of the tank, U_{bottom} is the heat transfer coefficient from the bottom surface, T_{tank} is tank temperature and $T_{\text{env, bottom}}$ is surrounding or environmental temperature at the bottom surface of the tank.

$$Q_{\text{loss, edge}} = A_{\text{edge}} U_{\text{edge}} (T_{\text{tank}} - T_{\text{env, edge}}) \quad (12)$$

where $Q_{\text{loss, edge}}$ shows the amount of energy lost from the edge of the tank, A_{edge} is the area of the edge surface of the tank, U_{edge} is the heat transfer coefficient from the edge surface, T_{tank} is tank temperature, and $T_{\text{env, edge}}$ is surrounding or environmental temperature at the edge surface of the tank.

Fig. 6 shows the enthalpy curve of the selected PCM. The main parameters needed to model the PCM tank are specific heat capacity during solid and liquid phases, thermal conductivity, temperature limits of the phase change, and heat of fusion. Equations (13) to (15) and Fig. 7 depict how the enthalpy changes with the material.

$$\text{if } T < T_{\text{low}} : h(T) = c_{p, \text{solid}} T \quad (13)$$

$$\text{if } T_{\text{low}} \leq T \leq T_{\text{up}} : h(T) = c_{p, \text{solid}} \cdot T_{\text{low}} + \text{PH} \cdot Q_{\text{Phase}} \text{ with } : \text{PH} \\ = (T - T_{\text{low}}) / (T_{\text{up}} - T_{\text{low}}) \quad (14)$$

$$\text{if } T > T_{\text{up}} : h(T) = c_{p, \text{solid}} \cdot T + Q_{\text{Phase}} + c_{p, \text{liquid}} \cdot (T - T_{\text{up}}) \quad (15)$$

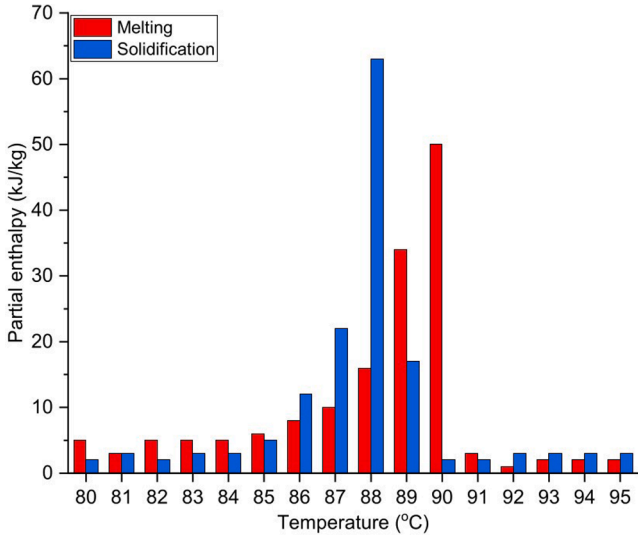


Fig. 6. Characterisation of enthalpy curve implemented in new TRNSYS PCM type.

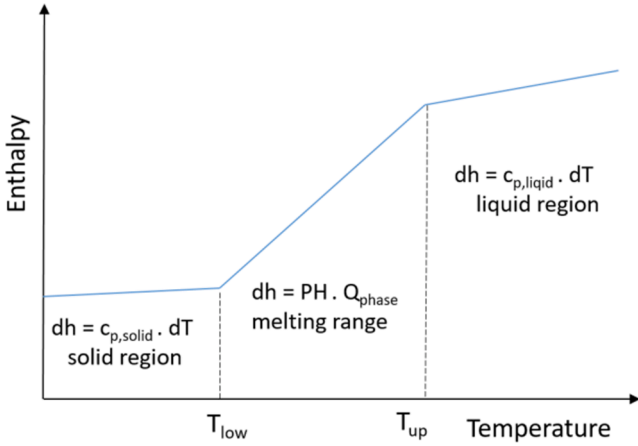


Fig. 7. Specific enthalpy $h(T)$ as a function of the material temperature.

For this study, the commercially available PCM based on Rubitherm SP90 was selected. This choice was primarily guided by its accessibility and characteristics, with high thermal storage capacity and low combustibility and assuming minimal variation in volume during the melting process. The chosen PCM has the potential to store up to 150 kJ/kg of energy within the temperature range between 88 and 90 °C. Thermal conductivity is essential to PCM integration since most PCMs have very low thermal conductivity, affecting the heat charging/discharging rate. Here, we considered an equivalent thermal conductivity of 5 W/m.K in tank integration, according to the various techniques found in the literature to improve the equivalent thermal conductivity, such as adding particles like copper powder [41], graphite powder [42], copper nanoparticles [43], embedding PCM into metallic foams [44], or utilising fins and matrices [45].

Hot water storage tank: The hot water tank was simulated using TRNSYS Type 156. Here, the tank was divided into ten *iso*-thermal temperature nodes to enhance thermal stratification, and an aspect ratio of 3.5 was selected to minimise thermal losses. The storage tank dissipates heat from the top, bottom, and edges while interacting with the environment. The detailed mathematical modelling of this component is similar to the PCM tank, with the heat capacity only driven by the sensible heat. More details can be found in the TRNSYS libraries [46].

3.2.2.3. Absorption chiller. TRNSYS Type 107 (available in the standard TRNSYS library) was chosen to model a hot water-operated absorption chiller. The specifications for the absorption chiller are presented in Table 4, and the performance charts for a single-stage absorption chiller are displayed in Fig. 8, collected from [47]. Based on these charts, external data files were established and integrated into TRNSYS. The data file comprises the ratio of the design energy and cooling capacity of the machine, which is determined by various factors such as hot water (HW), cooling water (CW), chilled water (CHW), and partial load conditions. Additional information regarding the mathematical modelling of this component can be found in the TRNSYS libraries [46].

3.2.2.4. Auxiliary boiler. TRNSYS Type 700 was used to simulate auxiliary gas boilers in the ACS model. This component provides supplementary energy and maintains the absorption chiller's operating temperature when solar irradiation is low. A thermostat (Type 108) regulates the operation of the auxiliary boiler.

3.2.2.5. Cooling tower. The cooling tower was modelled using TRNSYS Type 162. This type model counter flow forced draft cooling system, wherein hot water interacts directly with an air stream. More information regarding the mathematical modelling of this component can be found in the TRNSYS libraries [46].

3.2.2.6. Pumps. Variable flow rate pumps were modelled using TRNSYS Type 110. These pumps vary the flow rate depending on the control signal. The flow rate in the solar collector loop was changed by coupling Type 2b differential control with Type 22. The flow rate is adjusted based on the cooling demand profile in all other loops, including the HW, CW, and CHW.

3.2.3. System performance indicators

The performance of the investigated cooling systems was evaluated through the following indicators:

The solar fraction (SF) calculation - representing the proportion of energy derived from solar - was performed using the following equation (16).

$$SF = \frac{Q_{solar}}{Q_{solar} + Q_{aux}} \quad (16)$$

Where Q_{solar} is the amount of energy from solar while Q_{aux} denotes the energy from the auxiliary boiler.

The total primary energy consumption of the system was determined by factoring in the final energy consumption and primary energy factors. In the case of the ACS, electricity and natural gas are utilised to power various pumps and fans and boost hot water temperature in times of insufficient solar irradiance. On the other hand, the VCS system relies solely on electricity to operate its compressor, pumps, and fans. Mathematically, it can be expressed by equations (17) and (18) for ACS and VCS, respectively, according to [48].

$$PEC_{ACS} = (PEF_e \cdot E_e + PEF_{ng} \cdot E_{ng}) \quad (17)$$

$$PEC_{VCS} = (PEF_e \cdot E_e) \quad (18)$$

PEF represents the primary energy factor, subscript e for electricity, and ng for natural gas. The values of these factors for the investigated location are given in Table 5. E_e and E_{ng} are the yearly electricity and natural gas consumption, respectively.

Table 4
Solar-driven absorption chiller specifications.

	Hot water	Chilled water	Cooling water
Temperature in/out (°C)	90/85	12/7	29 /34
Flow rate (kg/hr)	4448	3024	7471

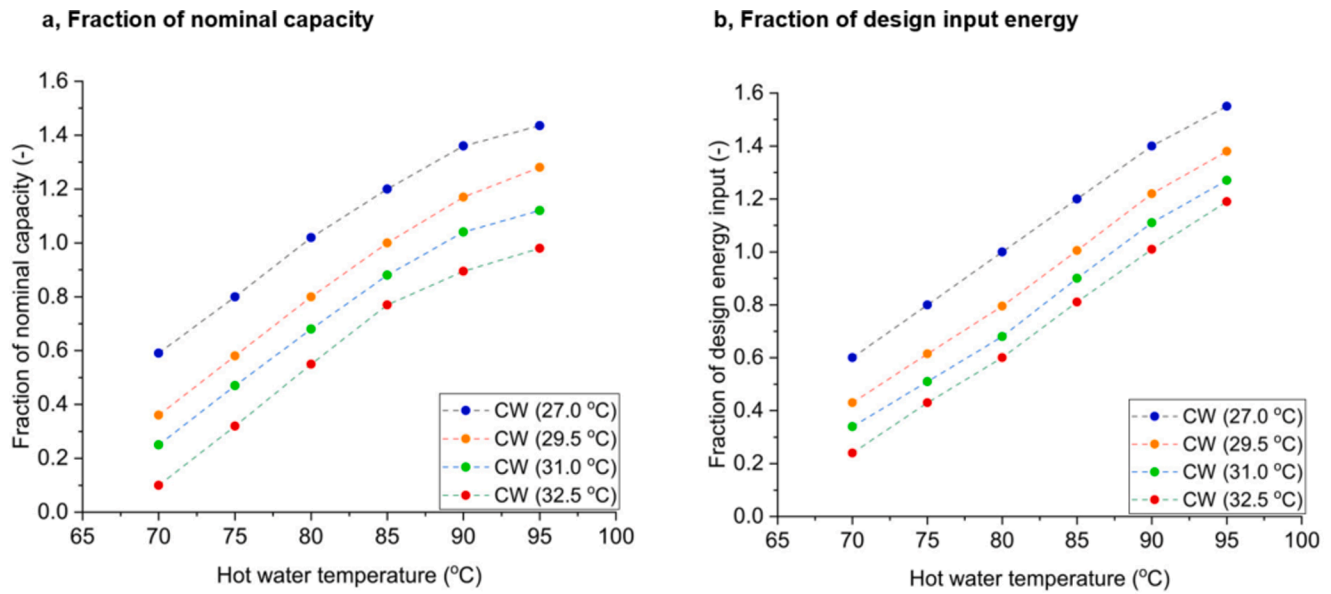


Fig. 8. Performance curves for a single-stage absorption chiller. a, Fraction of nominal capacity. b, The fraction of design input energy.

Table 5

Parameters considered for the energy and environmental assessment.

Parameter	Units	Amount
Electricity		
Average electricity price [50]	Rs./kWh	32.1
Primary energy factor for electricity [50]	kWh _{pe} /kWh _e	3.05
CO ₂ emission factor for electricity [51]	kg per MWh	566
Natural gas		
Average natural gas price [52]	Rs./kWh	8
Primary energy factor for natural gas [52]	kWh _{pe} /kWh _{ng}	1.22
CO ₂ emission factor for natural gas [51]	kg per MWh	202

The annual operating cost (fuel cost) for electricity and natural gas consumption can be calculated using equations (19) and (20).

$$FC_e = E_e \cdot c_e \quad (19)$$

$$FC_{ng} = E_{ng} \cdot c_{ng} \quad (20)$$

where FC_e and FC_{ng} are the annual cost of electricity and natural gas consumption; and c_e and c_{ng} are the unit cost of electricity and natural gas, respectively.

The total annual CO_{2eq} emissions (CDE) are the sum of emissions produced from electricity (CDE_e) and emissions from natural gas (CDE_{ng}) in the auxiliary boiler. These are given by

$$CDE = CDE_e + CDE_{ng} \quad (21)$$

$$CDE_e = E_e \cdot EF_{CO_2,e} \quad (22)$$

$$CDE_{ng} = E_{ng} \cdot EF_{CO_2,ng} \quad (23)$$

$EF_{CO_2,e}$ and $EF_{CO_2,ng}$ are CO_{2eq} emission factors for electricity and natural gas, listed in Table 5.

The formula for calculating LCC can be expressed as follows.

$$LCC = C_a + C_o + C_m \quad (24)$$

where C_a is the acquisition cost (initial purchase cost) of the cooling system, C_o is the operating costs (ongoing operational expenses) of the cooling system, and C_m is the maintenance costs (costs of maintaining, repairing, and servicing) of the cooling system.

First, the initial capital expenditure data was collected through a market survey, as tabulated in Table 6, to calculate the LCC. Secondly, annual operational costs were computed using TRNSYS simulation models. A 4.5 % annual escalation in energy pricing was assumed to calculate operational yearly expenses. The maintenance cost was considered to be 1.75 % of the capital for conventional vapour compression cooling systems and 1.25 % for absorption cooling systems, according to [48]. The currency of reference for the selected case study was the Pakistani rupee, and the projected lifespan of the system was set at 25 years, according to manufacturer reports and published literature [48,49]. The performance of all the components was assumed to be constant over the years.

3.2.4. Model validation and limitations

This study integrates two numerical models associated with a residential building archetype to generate an hourly cooling demand profile, and a solar-driven ACS to simulate the renewable cooling supply capacity.

The numerical building of the residential building archetype was already validated in a previous study [3]. The model was validated following the ASHRAE standard 14-2014 using monthly energy data [3]. The Normalized Mean Bias Error (NMBE), the Coefficient of Variation of the Root Mean Square Error (CV-RMSE), and the coefficient of determination were employed as uncertainty indices for the validation (R^2). An NMBE of 3.3 %, a CV-RMSE of 9.1 %, and an R^2 of 0.9 were found when measured and simulated values were compared.

The numerical model of the solar-driven absorption cooling technology is based on the TRNSYS Type 107, which has been widely used in the literature [53–55]. The performance data for the absorption chiller were gathered from [47], while solar collector data was collected from

Table 6

Capital cost functions of main components (in Pakistani Rupees) [49].

Parameter	Cost function (Pakistani Rupees)
ETC collector	250,000 per m ²
Auxiliary boiler	110,000 per kW
Vapour compression system	25,568 per kW
Pump	6000 per kW
Hot water storage tank	40,000 per m ³
PCM water storage tank	80,000 per m ³
Single-effect absorption chiller	31,250 per kW
Cooling tower	2840 per kW

the manufacturer report [56]. The thermal efficiency curve of the collector, obtained from the simulation model, was compared with the manufacturer's reported data, and differences of less than 2 % were observed. The numerical model for latent heat storage using different PCMs has also been tested and verified in previous studies [29,38]. The thermophysical properties of the system were defined using real material characteristics, and consistency criteria in latent heat energy balance were applied.

It should be noted that no experimental results were used to validate the whole integration, which generate uncertainty regarding the final absolute performance of systems. However, the research findings are based on model comparison under similar assumptions and boundary

conditions, ensuring the representativeness of the comparisons. Moreover, a parametric analysis was developed to highlight critical criteria for optimal implementation.

For the LCC assessment, the performance of the components was assumed to be constant over the years.

4. Results and discussion

This section shows the result and discussion of solar-driven ACS with two different TES and a comparison with electric-driven vapour compression technology. It is divided into five sections. First, the cooling demand profile and system sizing are introduced (Section 4.1). Second, a

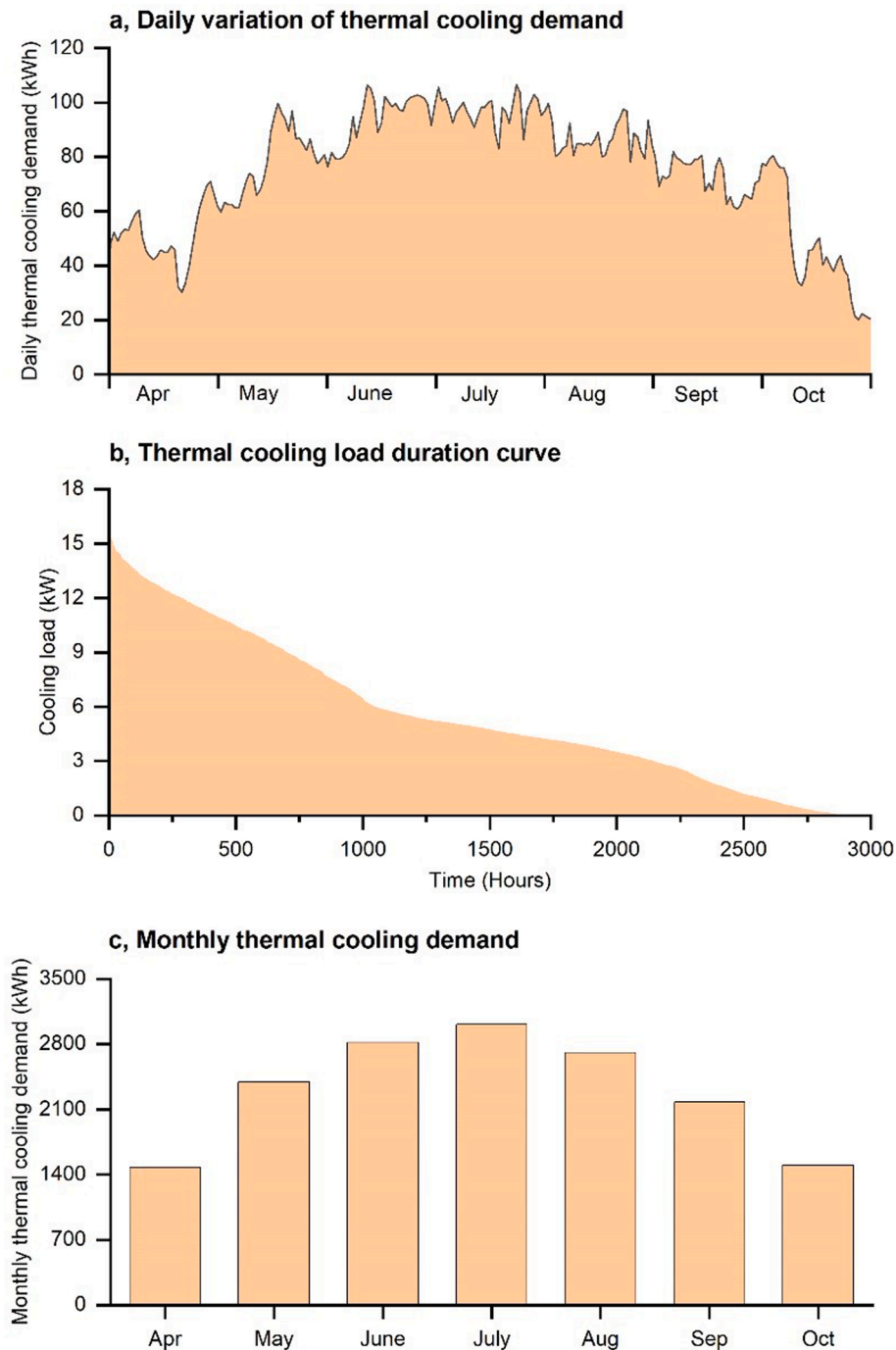


Fig. 9. Analysis of the thermal cooling demand profile. a, Daily variation of thermal cooling demand. b, Thermal cooling load duration curve. c, Monthly thermal cooling demand.

parametric analysis is developed to identify the optimal configuration of the PCM-based ACS integration and the conventional ACS using sensible heat storage (Section 4.2). Third, the performance of the PCM-based solar-driven ACS is compared to a conventional solar-driven ACS (Section 4.3). Fourth, the performance of the proposed PCM-based solar-driven ACS is compared with a VCS (Section 4.4). Finally, the LCC of the three different cooling alternatives is compared and discussed (Section 4.5).

4.1. Cooling demand profile and system sizing

This first section discusses the residential case study's cooling demand profile and system sizing. Fig. 9 shows the variation of daily thermal cooling demand throughout the hot season (a), the thermal cooling load duration curve for system sizing (b), and monthly thermal cooling needs (c).

The cooling demand of a building exhibits temporal variability, occurring on a daily and yearly basis. Fig. 9(a) illustrates the daily

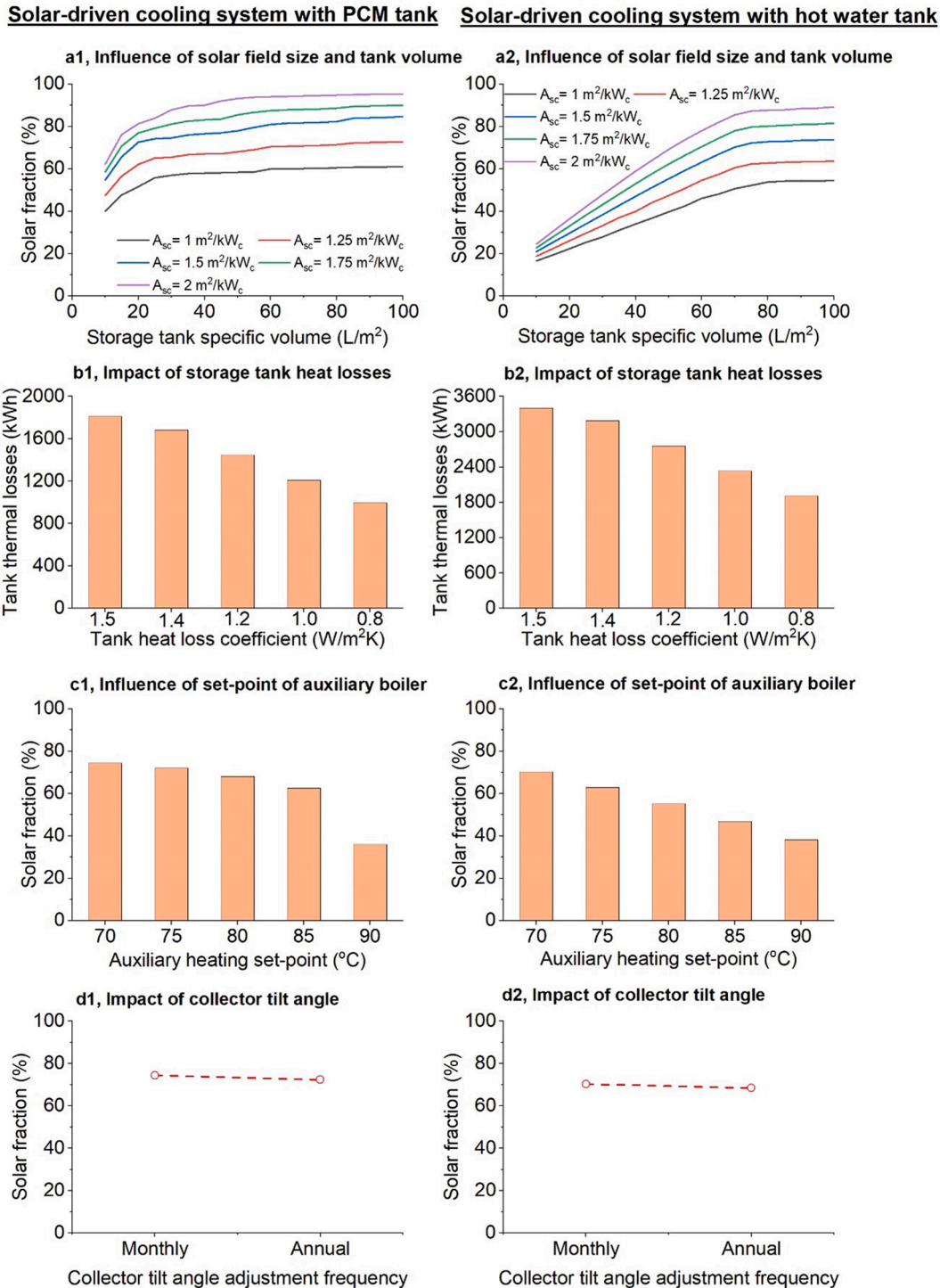


Fig. 10. Parametric study of the solar-driven cooling system with PCM tank (a) and hot water tank (b); (a1,a2) Influence of solar field size and tank volume; (b1,b2) Impact of storage tank heat losses; (c1,c2) Influence of auxiliary system set-point temperature; (d1,d2) Implications of collector tilt angle and its adjustment frequency.

thermal cooling demand variations (daily kWh) throughout the selected timeframe. Days with the highest daily cooling needs are found in June and July. Specifically, the analysis identified the highest daily cooling demand of 106.5 kWh in July, with hourly peak demand during the daytime. Fig. 9(b) provides the load duration curve (cooling capacity, in kW). The maximum thermal cooling capacity required for the residential building under analysis is 15.9 kW. Fig. 9(c) illustrates the monthly variations in the building's thermal demand, highlighting a significant monthly change in cooling demand, with the lowest consumption of 1478 kWh in April; and experiencing the highest cooling demand of 3013 kWh in July. The total annual cooling demand of the investigated building was found to be 16,088 kWh (175.4 kWh/m²).

4.2. Parametric analysis of PCM integration for solar-driven absorption cooling technology

In this section, a parametric study is performed to identify the optimal sizing of the solar-driven ACS regarding the solar field size, storage tank volume, tank insulation, auxiliary boiler set-point temperature, and collector tilt angle with or without monthly adjustments. Fig. 10 summarises the parametric study results with the PCM tank (Fig. 10a1-d1) and hot water tank (Fig. 10a2-d2).

Fig. 10 (a1,a2) depicts the changes in solar fraction with variations in solar field size (m²) and the storage tank volume (m³), considering a tank heat loss coefficient of 0.8 W/m².K. In this analysis, the solar field size was selected according to cooling demand and storage tank sizes were selected based on the solar field. The analysis covers solar field sizes ranging from 1 to 2 m²/kW_e, and storage tank volumes from 10 to 100 L/m². The findings show that solar fraction increases with the collector area of both systems. However, the impact is limited by the cooling demand profile, and therefore, adding more collector area to achieve a higher solar fraction does not result in significant improvements. Comparing the volume ranges, the shorter range in PCM volume to achieve a high solar fraction is associated with a higher TES density. The solar fraction increase rate difference in both scenarios is associated with the sensible and latent heat storage phases. It can be noted that a higher increase in PCM volume doesn't provide a continued (or constant) increase in solar fraction. This is associated with the lower operating conditions of the tank, decreasing the use of the phase change and its latent heat capacity.

Conversely, increasing the thermal energy storage volume enhances the solar fraction of all configurations up to a point from which it remains almost constant. As a result, exceeding a specific thermal energy storage volume would not yield any additional benefits. Based on the analysis, it is found that the ACS configuration with a PCM tank should have a tank volume of approximately 30 L/m². A tank volume of 75 L/m² would be more suitable for the ACS configuration with a water tank.

Fig. 10(b1,b2) shows the performance of both systems by varying the storage tank's heat loss coefficient (U-value, W/m².K). The U-value was changed from 0.8 to 1.5 W/m².K to represent various insulation levels ranging from an insulated tank to a poorly insulated one. The results show a significant increase in tank losses in poorly insulated scenarios, reducing the solar fraction. Furthermore, excessive heat losses from the tank can cause de-stratification and adversely affect the overall absorption chiller performance. Therefore, it is crucial to properly insulate the tank to mitigate tank thermal losses and enhance the performance of the ACS. Based on these findings, a U-value of 0.8 is chosen for both TES.

Fig. 10(c1, c2) investigates how the solar fraction varies with different auxiliary boiler set-point temperatures. The findings indicate that a higher set-point temperature for the auxiliary boiler results in a lower solar fraction. This occurs because a higher set-point temperature leads to more energy supplied by the auxiliary boiler. Thus, selecting an appropriate set-point temperature is critical in ensuring optimal system performance and maximising renewable cooling supply.

The analysis also shows the importance of a right tilt angle to ensure maximum solar irradiance and maximise the solar fraction. For a fixed

annual adjustment, a tilt angle of 27 degrees resulted in the highest solar irradiance. However, changing the collector tilt angle on a monthly basis resulted in a significant impact, increasing solar fraction by up to 2.1 % for both systems (Fig. 10d1,d2).

This optimal monthly collector title angle varies, as shown in Fig. 11. A higher tilt angle is required in winter, while a lower angle is needed in summer, with the peak summer angle being close to zero degrees. This monthly adjustment approach provides a cost-effective alternative to expensive tracking systems for thermal collectors.

Based on this parametric analysis, the optimal configuration for both systems - ACS with PCM and hot water tanks - has been selected. The solar field size of 1.5 m²/kW_e, storage volumes of 30 L/m² for the PCM tank and 75 L/m² for the hot water tank, and tank heat loss coefficient of 0.8 W/m².K have been chosen. In addition, the auxiliary set-point of 70 °C and the monthly optimum collector angle have been selected. By implementing this optimal configuration in both systems, the following section analyses the specific benefits of the PCM integration to maximise the performance of the ACS.

4.3. Performance of solar-driven absorption cooling system with and without PCM

This section compares the thermal performance of solar-driven ACS integrating latent heat storage (PCM tank) with the conventional integration based on sensible heat storage (hot water tank), following the optimal configurations previously discussed.

The monthly performance of ACS equipped with PCM is tabulated in Table 7. The data shows that the collector generates useful heat between 2564 and 3058 kWh, with a monthly collector efficiency ranging from 45.8 % to 56.6 %. Meanwhile, the PCM tank experiences heat losses ranging from 132 to 180 kWh, with the most significant losses occurring in April and October due to the lower ambient temperatures. The auxiliary energy requirements for the system range from 52 kWh to 2029 kWh per month, with lower energy requirements in April and October due to reduced cooling needs. The monthly solar fraction, representing the proportion of total cooling provided by solar energy, varies from 61 % to 95.8 %.

Table 8 summarises the monthly thermal performance of ACS integrated with a water tank. The findings indicate that the collector generates useful heat, ranging from 2430 to 2839 kWh, with a monthly collector efficiency between 44.1 % and 52.6 %. The hot water tank also experiences heat losses between 246 and 316 kWh, with the most substantial losses occurring in April and October due to lower ambient temperatures. The system's auxiliary energy requirements range from 273 kWh to 2221 kWh per month, with lower energy needs in April and October due to reduced cooling demands. Moreover, the monthly solar fraction with this configuration ranges from 56.6 % to 92.2 %.

Fig. 12 compares the annual performance of both solar-driven cooling systems with PCM and hot water tanks.

The results demonstrate how the PCM tank integration improves the thermal performance of the solar-driven ACS. The tank's capacity to store thermal energy at a higher density and provide higher temperature outputs resulted in a substantial increase in the solar fraction. The heat losses under similar boundary conditions are mitigated by 44 % (from 1909 to 1071 kWh). The results demonstrate how the PCM tank can maximise the solar fraction by 4.2 % compared to a conventional ACS (from 70.3 to 74.5 %) and reduce the auxiliary energy needed to run the ACS from 9412 to 7792 kWh.

4.4. Performance of solar-driven absorption cooling system with vapour compression technology

In this section, the performance of the solar-driven ACS with a PCM tank is compared with a VCS based on economic, energy and environmental indices. A vapour compression unit for the same case study was sized and numerically evaluated under similar boundary conditions. The

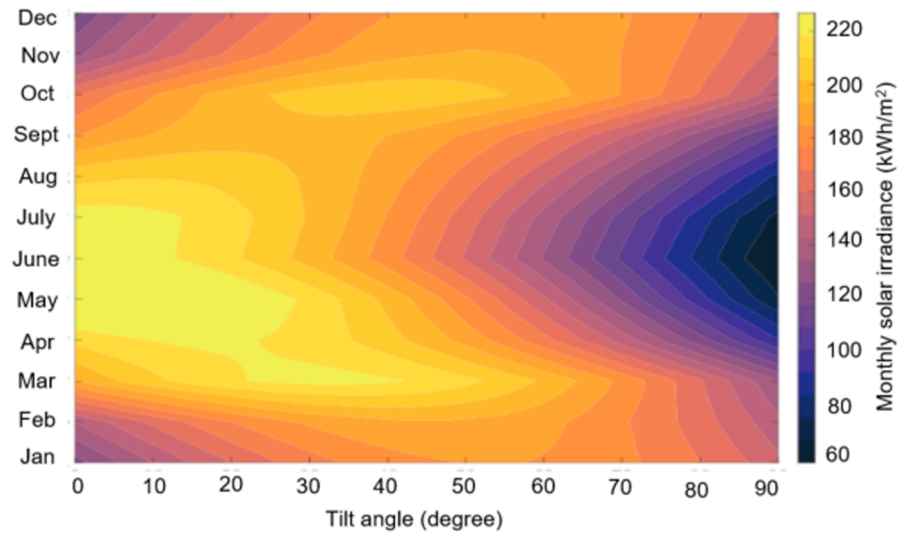
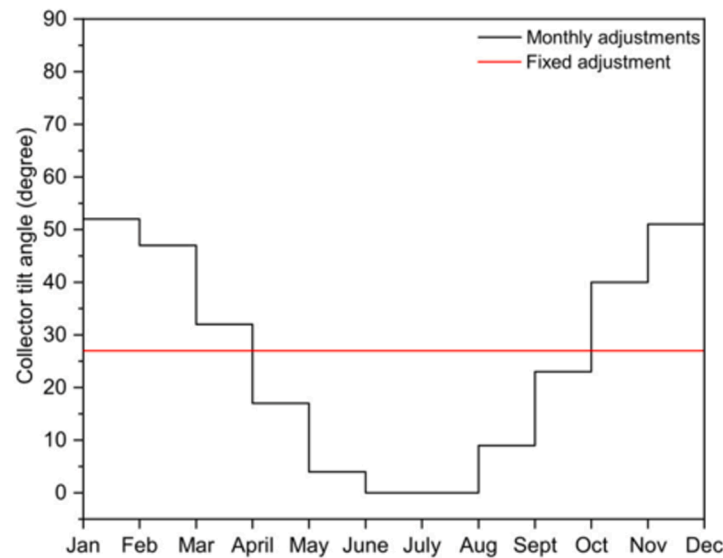
a, Monthly solar irradiance as a function of collector tilt angle**b, Optimal annual and monthly values of the collector tilt angle**

Fig. 11. Analysis of solar irradiance and collector tilt angle. a, Variation of monthly solar irradiance at the collector surface in an extremely hot region (Sukkur) as a function of collector tilt angle. b, Optimal annual and monthly values of the collector tilt angles.

Table 7

Monthly performance of absorption chiller with PCM tank.

Month	Solar irradiance (kWh)	Collector energy (kWh)	Auxillary energy (kWh)	Tank losses (kWh)	Collector efficiency	Solar fraction
April	5721	2622	52	168	45.8 %	95.8 %
May	5801	2995	1068	145	51.6 %	72.9 %
June	5329	2985	1696	132	56.0 %	63.4 %
July	5398	3058	2029	142	56.6 %	61.0 %
August	5345	2964	1616	149	55.4 %	65.0 %
September	5244	2704	996	154	51.6 %	71.8 %
October	5374	2564	335	180	47.7 %	91.8 %
Total/Average	38,212	19,892	7792	1071	52.1 %	74.5 %

energy and environmental performance are compared using primary energy consumption (PEC) and kg of CO_{2eq} emissions of both integrations. The economic analysis focuses on each system's initial investment and operating costs. Fig. 13 shows both systems' monthly PEC and kg of CO_{2eq} emissions.

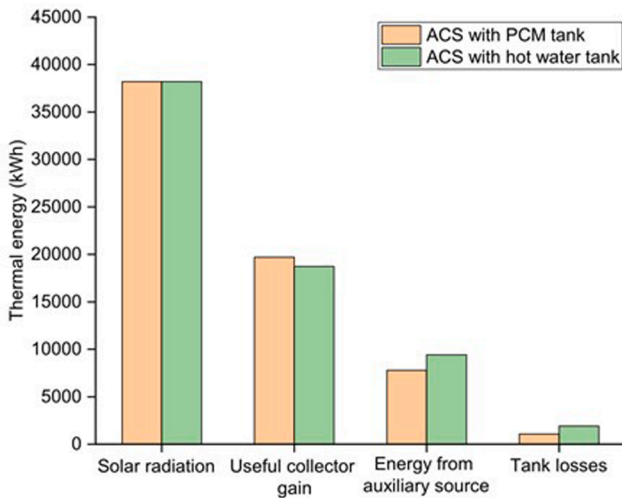
It is found that the monthly PEC of the VCS varies between 1358 and

3494 kWh, whereas the PCM-based solar-driven ACS system's primary energy consumption ranges between 381 and 2870 kWh. The maximum primary energy savings are observed in April, May, and June due to the higher solar fraction in the solar-driven ACS system. Similarly, the monthly kg of CO_{2eq} emissions for the VCC system ranges from 252 to 648 kg of CO_{2eq}, while the ACS system ranges between 69 and 483 kg of

Table 8

Monthly performance of absorption chiller with a water tank.

Month	Solar irradiance (kWh)	Collector energy (kWh)	Auxiliary energy (kWh)	Tank losses (kWh)	Collector efficiency	Solar fraction
April	5721	2523	273	287	44.1 %	92.2 %
May	5801	2807	1343	261	48.4 %	68.4 %
June	5329	2740	2008	246	51.4 %	58.2 %
July	5398	2839	2221	257	52.6 %	56.6 %
August	5345	2786	1839	269	52.1 %	61.1 %
September	5244	2601	1241	273	49.6 %	69.0 %
October	5374	2430	487	316	45.2 %	86.9 %
Total/Average	38,212	18,726	9412	1909	49.1 %	70.3 %

**Fig. 12.** Seasonal thermal energy availability of solar-driven cooling system with PCM and hot water tank.

$\text{CO}_{2\text{eq}}$. These findings show how solar-driven ACS with a PCM tank can reduce $\text{CO}_{2\text{eq}}$ emissions and offer a more environmentally friendly cooling option than the VCS system.

Table 9 summarises the key metrics, including the initial investment cost, operating cost, final energy consumption, primary energy consumption, and $\text{CO}_{2\text{eq}}$ emissions for both systems.

The analysis reveals that the solar-driven ACS with a PCM tank is considerably more expensive than the VCS system, with an initial capital investment cost that is 212 % higher. Specifically, the solar-driven ACS

system requires an initial investment of 14.0×10^5 Pakistani rupees, whereas the VCS system costs only 4.5×10^4 . However, the seasonal running cost of the ACS system is 52 % lower than the VCS system due to its lower PEC. The PCM-based solar-driven ACS system could save 31.6 % (5562 kWh) of primary energy each year to fulfil the cooling requirement.

Comparing the environmental impacts of both systems shows that the PCM-based solar-driven ACS system would result in annual emissions of 2042 $\text{kgCO}_{2\text{eq}}$ for the selected building, while the VCS system would lead to higher emissions of 3265 $\text{kgCO}_{2\text{eq}}$. The solar-driven cooling system with a PCM tank could save 1223 $\text{kgCO}_{2\text{eq}}$ emissions annually. These results highlight additional criteria to support the decision making process towards sustainable cooling alternatives for buildings.

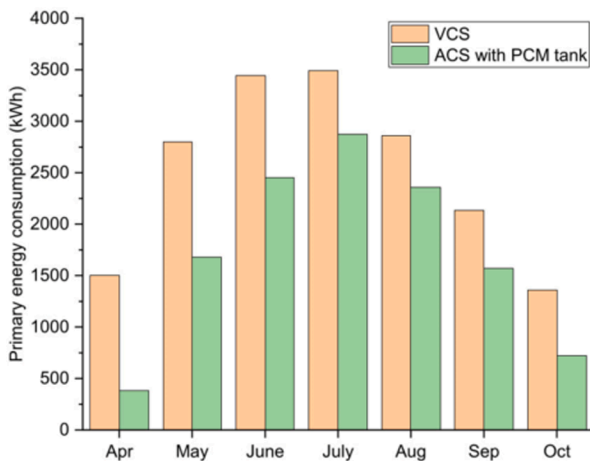
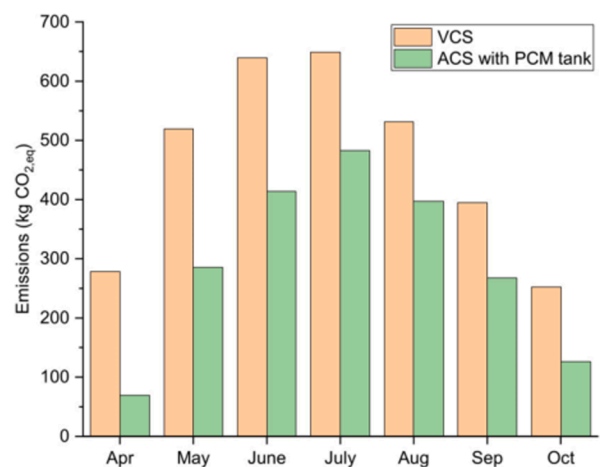
4.5. Life cycle cost analysis

This section compares the LCC of the PCM-based solar-driven ACS with a conventional solar-driven ACS and an electric-driven VCS. The

Table 9

Comparison of the PCM-based solar-driven ACS and VCC systems.

	ACS system with PCM tank	VCC system
Initial capital investment cost (Rs.)	1,404,384	450,000
Annual operating cost (Rs.)	88,906	185,157
Annual final energy consumption (kWh)	828 (electricity) + 7792 (gas)	5768 (electricity)
Annual primary energy consumption (kWh)	12,031	17,593
Annual emissions (kg of $\text{CO}_{2\text{eq}}$)	2042	3265

a, Comparison of monthly primary energy consumption**b, Comparison of monthly $\text{CO}_{2\text{eq}}$ emissions****Fig. 13.** Comparison between the PCM-based solar-driven ACS and a vapour compression technology. a, Monthly primary energy consumption (kWh). b, Monthly carbon emission ($\text{kgCO}_{2\text{eq}}$).

analysis includes the costs associated with initial investment, operation, and maintenance over the expected lifespan of each system.

Fig. 14 illustrates the LCC analysis outcomes for the three systems. The operational year is depicted on the x-axis, while the y-axis represents the accumulated LCC. Through a comparison of these costs, it can be determined which system offers the most sustainable and cost-effective cooling solution based on the operational years considered.

The initial cost of a solar-driven ACS with a PCM tank is higher than that of a VCS system. However, the lower operating costs of the PCM-based solar-driven ACS over time make its total cost more favourable than that of the VCS. Now, comparing the initial cost of solar-driven ACS with PCM and hot water tank, both systems are similar. Although the unit cost of the PCM tank is higher, its smaller size offsets the higher cost. Additionally, the ACS with a PCM tank provides monetary benefits from the 9th year, earlier than the ACS with a hot water tank, which requires two additional years due to its higher auxiliary energy requirements.

According to the LCC analysis, when taking into account a 25-year lifespan, the solar-driven ACS equipped with a PCM tank incurs 34 % lower costs than the VCS system and 9 % lower costs than the conventional ACS. These results suggest that the solar-driven ACS with PCM is more sustainable and cost-effective over the long term than the other two systems. These results highlight the importance of considering immediate requirements, long-term sustainability, and cost-effectiveness when selecting a cooling system.

5. Conclusions

This study analyses the benefits of latent heat storage to improve the performance of solar-driven absorption cooling for residential applications in extremely hot dry climates. The optimal integration is identified and compared with a conventional solar-driven absorption cooling system and an electric-driven vapour compression technology. The energy, environmental and economic performance of technologies were compared through a dynamic simulation model using TRNSYS software in a residential case study in Pakistan. The following conclusions are drawn.

- 1) The results demonstrate how latent heat storage increases the solar fraction of solar-driven absorption cooling by 4.2 % (from 70.3 to 74.5 %) compared with the optimal conventional integration using sensible heat storage. The PCM can reduce tank heat losses by 44 % (from 1909 to 1071 kWh) due to the higher heat storage density and lower storage volume.
- 2) The optimisation of the PCM-based solar-driven cooling system highlights that a solar field size of $1.5 \text{ m}^2/\text{kW}_c$, combined with a specific PCM storage tank of 30 L/m^2 , and adequate insulation below $0.8 \text{ W/m}^2\cdot\text{K}$ provided the optimal configuration. The analysis also shows how solar fraction drastically changes by varying the auxiliary boiler set-point temperature. Higher set-point temperatures reduce the solar fraction, as they hinder the thermal energy storage tank from absorbing all the energy from the solar field.
- 3) Comparing the PCM-based solar-driven cooling system with the electric-driven vapour compression system revealed that although the former has a 212 % higher initial cost (from 450,000 to 1,403,484 Rs.), the operating cost can be reduced by 52 % (from 185,157 to 88,906 Rs.). Moreover, in the specific case study, the solar-driven absorption cooling system reduced primary energy consumption by 31.6 % (from 17,593 to 12,031 kWh) and mitigated carbon emissions by 37.4 % (from 3265 to 2042 kgCO_{2eq}) annually.
- 4) Despite the higher initial investment cost of PCM-based solar-driven cooling, the findings also show that the life cycle cost is much lower in extremely hot dry climates. After 25 years, the LCC is lowered by 34 % compared to vapour compression and by 9 % compared to a conventional solar-driven cooling system using a hot water tank.

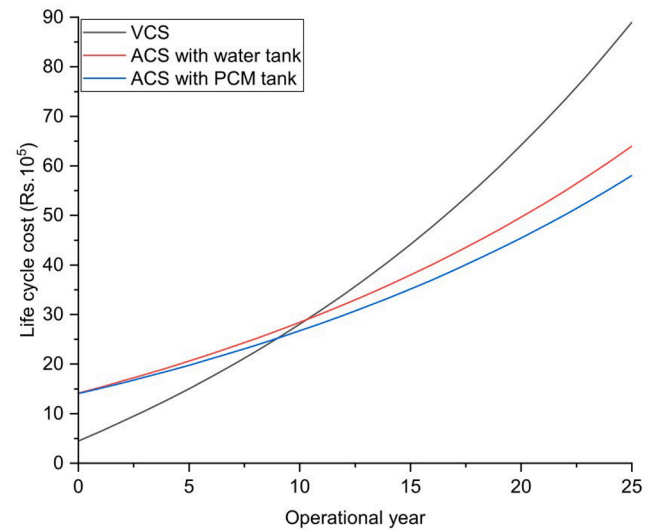


Fig. 14. Life cycle cost analysis comparing the PCM-based solar-driven ACS with a conventional ACS and vapour compression cooling system.

This paper provides valuable recommendations and key strategies to improve the energy, environmental and economic performance of solar-driven absorption cooling for extremely hot climates. The findings demonstrate the benefits of solar cooling technologies for areas with high solar radiation and high cooling demand.

CRediT authorship contribution statement

Sajid Mehmood: Conceptualization, Methodology, Software, Validation, Investigation, Data curation, Writing – original draft, Visualization, Project administration, Funding acquisition. **Jesus Lizana:** Conceptualization, Methodology, Investigation, Writing – review & editing, Project administration, Funding acquisition. **Daniel Friedrich:** Conceptualization, Methodology, Writing – review & editing, Project administration, Funding acquisition.

Declaration of Competing Interest

The authors declare that they have no known competing financial interests or personal relationships that could have appeared to influence the work reported in this paper.

Data availability

Data will be made available on request.

Acknowledgements

This research has received financial support from the Higher Education Commission of Pakistan, the University of Engineering and Technology, Lahore, New Campus, Pakistan, and the UK ESRC Cool infrastructure project (ES/T008091/1). The work was also supported by the European Union's Horizon 2020 research and innovation programme under the Marie Skłodowska-Curie grant agreement No 101023241.

References

- [1] Miranda N, Lizana J, Sparrow S, Zachau-walker M, Watson P, Wallom D, et al. Change in cooling degree days with global mean temperature increasing from 1.5° to 2.0°C. *Nat Sustain* 2023. <https://doi.org/10.1038/s41893-023-01155-z>.
- [2] IEA. The Future of Cooling: Opportunities for energy-efficient air conditioning 2018:92. <https://www.iea.org/reports/the-future-of-cooling>.

- [3] Mehmood S, Lizana J, Núñez-Peiró M, Maximov SA, Friedrich D. Resilient cooling pathway for extremely hot climates in southern Asia. *Appl Energy* 2022;325. <https://doi.org/10.1016/j.apenergy.2022.119811>.
- [4] Shahid M, Ullah K, Imran K, Mahmood I, Mahmood A. Electricity supply pathways based on renewable resources: A sustainable energy future for Pakistan. *J Clean Prod* 2020;263:121511. <https://doi.org/10.1016/j.jclepro.2020.121511>.
- [5] Lizana J, Miranda ND, Gross L, Mazzone A, Cohen F, Palafox-Alcantar G, et al. Overcoming the incumbency and barriers to sustainable cooling. *Build Cities* 2022; 3:1075–97. <https://doi.org/10.5334/bc.255>.
- [6] Ibrahim NI, Al-Sulaiman FA, Saidur R. Performance assessment of water production from solar cooling system in humid climate. *Energy Convers Manag* 2016;127:647–55. <https://doi.org/10.1016/j.enconman.2016.09.056>.
- [7] Ford B, Mumovic D, Rawal R. Alternatives to air-conditioning: policies, design, technologies, behaviours. *Build Cities* 2022;3:433–47. <https://doi.org/10.5334/bc.256>.
- [8] Shirazi A, Taylor RA, Morrison GL, White SD. Solar-powered absorption chillers: A comprehensive and critical review. *Energy Convers Manag* 2018;171:59–81. <https://doi.org/10.1016/j.enconman.2018.05.091>.
- [9] Siddiqui MU, Said SAM. A review of solar powered absorption systems. *Renew Sustain Energy Rev* 2015;42:93–115. <https://doi.org/10.1016/j.rser.2014.10.014>.
- [10] Sarbu I, Sebarchievici C. General review of solar-powered closed sorption refrigeration systems. *Energy Convers Manag* 2015;105:403–22. <https://doi.org/10.1016/j.enconman.2015.07.084>.
- [11] Khan MSA, Badar AW, Talha T, Khan MW, Butt FS. Configuration based modeling and performance analysis of single effect solar absorption cooling system in TRNSYS. *Energy Convers Manag* 2018;157:351–63. <https://doi.org/10.1016/j.enconman.2017.12.024>.
- [12] Angrisani G, Entchev E, Roselli C, Sasso M, Tiarillo F, Yaici W. Dynamic simulation of a solar heating and cooling system for an office building located in Southern Italy. *Appl Therm Eng* 2016;103:377–90. <https://doi.org/10.1016/j.applthermaleng.2016.04.094>.
- [13] Bellos E, Tzivanidis C, Antonopoulos KA. Exergetic, energetic and financial evaluation of a solar driven absorption cooling system with various collector types. *Appl Therm Eng* 2016;102:749–59. <https://doi.org/10.1016/j.applthermaleng.2016.04.032>.
- [14] Tashtoush B, Alshare A, Al-Rifai S. Hourly dynamic simulation of solar ejector cooling system using TRNSYS for Jordanian climate. *Energy Convers Manag* 2015; 100:288–99. <https://doi.org/10.1016/j.enconman.2015.05.010>.
- [15] Bellos E, Tzivanidis C, Antonopoulos KA. Exergetic and energetic comparison of LiCl-H₂O and LiBr-H₂O working pairs in a solar absorption cooling system. *Energy Convers Manag* 2016;123:453–61. <https://doi.org/10.1016/j.enconman.2016.06.068>.
- [16] Gunhan T, Ekren O, Demir V, Hepbasli A, Ereik A, Sahin AS. Experimental exergetic performance evaluation of a novel solar assisted LiCl-H₂O absorption cooling system. *Energy Buildings* 2014;68:138–46. <https://doi.org/10.1016/j.enbuild.2013.09.025>.
- [17] She X, Yin Y, Xu M, Zhang X. A novel low-grade heat-driven absorption refrigeration system with LiCl-H₂O and LiBr-H₂O working pairs. *Int J Refrig* 2015; 58:219–34. <https://doi.org/10.1016/j.ijrefrig.2015.06.016>.
- [18] Shirazi A, Pintaldi S, White SD, Morrison GL, Rosengarten G, Taylor RA. Solar-assisted absorption air-conditioning systems in buildings: Control strategies and operational modes. *Appl Therm Eng* 2016;92:246–60. <https://doi.org/10.1016/j.applthermaleng.2015.09.081>.
- [19] Atmaca I, Yigit A. Simulation of solar-powered absorption cooling system. *Renew Energy* 2013;28:1277–93. [https://doi.org/10.1016/s0960-1481\(02\)00252-5](https://doi.org/10.1016/s0960-1481(02)00252-5).
- [20] Al-Alili A, Hwang Y, Rademacher R, Kubo I. Optimization of a solar powered absorption cycle under Abu Dhabi's weather conditions. *Sol Energy* 2010;84: 2034–40. <https://doi.org/10.1016/j.solener.2010.09.013>.
- [21] Altun AF, Kilic M. Economic feasibility analysis with the parametric dynamic simulation of a single effect solar absorption cooling system for various climatic regions in Turkey. *Renew Energy* 2020;152:75–93. <https://doi.org/10.1016/j.renene.2020.01.055>.
- [22] Buonomo B, Casaccia F, Cirillo L, Nardini S. Application of nanofluids in solar cooling system: Dynamic simulation by means of TRNSYS software. *Model Meas Control B* 2018;87:143–50. <https://doi.org/10.18280/mmc-b.870305>.
- [23] Habib MF, Ali M, Sheikh NA, Badar AW, Mehmood S. Building thermal load management through integration of solar assisted absorption and desiccant air conditioning systems: A model-based simulation-optimisation approach. *J Build Eng* 2020;30:101279. <https://doi.org/10.1016/j.jobe.2020.101279>.
- [24] Nienborg B, Dalibard A, Schnabel L, Eicker U. Approaches for the optimised control of solar thermally driven cooling systems. *Appl Energy* 2017;185:732–44. <https://doi.org/10.1016/j.apenergy.2016.10.106>.
- [25] Lizana J, Chacartegui R, Barrios-Padura A, Valverde JM. Advances in thermal energy storage materials and their applications towards zero energy buildings: A critical review. *Appl Energy* 2017;203:219–39. <https://doi.org/10.1016/j.apenergy.2017.06.008>.
- [26] Lizana J, Chacartegui R, Barrios-Padura A, Ortiz C. Advanced low-carbon energy measures based on thermal energy storage in buildings: A review. *Renew Sustain Energy Rev* 2018;82:3705–49. <https://doi.org/10.1016/j.rser.2017.10.093>.
- [27] Biarreau LT, Davis LW, Gertler P, Wolfram C. Heat exposure and global air conditioning. *Nat Sustain* 2020;3:25–8. <https://doi.org/10.1038/s41893-019-0441-9>.
- [28] Beck HE, Zimmermann NE, McVicar TR, Vergopolan N, Berg A, Wood EF. Present and future köppen-geiger climate classification maps at 1-km resolution. *Sci Data* 2018;5:1–12. <https://doi.org/10.1038/sdata.2018.214>.
- [29] Lizana J, Bordin C, Rajabloo T. Integration of solar latent heat storage towards optimal small-scale combined heat and power generation by Organic Rankine Cycle. *J Energy Storage* 2020;29:101367. <https://doi.org/10.1016/j.est.2020.101367>.
- [30] Lizana J, Sanchez-Jimenez PE, Chacartegui R, Becerra JA, Perez-Maqueda LA. Supercooled sodium acetate aqueous solution for long-term heat storage to support heating decarbonisation. *J Energy Storage* 2022;55:105584. <https://doi.org/10.1016/j.est.2022.105584>.
- [31] Lizana J, Perejón A, Sanchez-Jimenez PE, Perez-Maqueda LA. Advanced parametrisation of phase change materials through kinetic approach. *J Energy Storage* 2021;44:103441. <https://doi.org/10.1016/j.est.2021.103441>.
- [32] Lizana J, Chacartegui R, Barrios-Padura A, Valverde JM, Ortiz C. Identification of best available thermal energy storage compounds for low-to-moderate temperature storage applications in buildings. *Mater Construcción* 2018;68:1–35. <https://doi.org/10.3989/mc.2018.10517>.
- [33] Mehmood S, Lizana J, Friedrich D. Low-energy resilient cooling through geothermal heat dissipation and latent heat storage. *J Energy Storage* 2023;72: 108377. <https://doi.org/10.1016/j.est.2023.108377>.
- [34] Repository of free climate data for building performance simulation n.d. <https://climate.onebuilding.org/> (accessed February 7, 2021).
- [35] ISO 13790:2008 - Energy performance of buildings — Calculation of energy use for space heating and cooling n.d. <https://www.iso.org/standard/41974.html> (accessed February 24, 2022).
- [36] EN 15242, EN 15242:2007. Ventilation for buildings. Calculation methods for the determination of air flow rates in buildings including infiltration; 2007. <http://vdocuments.net/en-15242pdf.html?page=1> (accessed May 24, 2022).
- [37] Solar Energy Laboratory Univ. of Wisconsin-Madison, GmbH TE, Specialists CS et T du BES. Trnsys 18, a TRnsient SYstem Simulation program: Volume 4 Mathematical Reference 2018;4:705.
- [38] Lizana J, Friedrich D, Renaldi R, Chacartegui R. Energy flexible building through smart demand-side management and latent heat storage. *Appl Energy* 2018;230: 471–85. <https://doi.org/10.1016/j.apenergy.2018.08.065>.
- [39] Streicher W, Bony J, Citherlet S, Heinz A, Puschner P, Schranzhofer H, et al. Simulation models of PCM storage units. A Report of IEA Solar Heating and Cooling programme - Task 32 "Advanced storage concepts for solar and low energy buildings". Report C5 of Subtask C 2008.
- [40] Bony J, Citherlet S. Numerical model and experimental validation of heat storage with phase change materials. *Energy Buildings* 2007;39:1065–72. <https://doi.org/10.1016/j.enbuild.2006.10.017>.
- [41] Jinfeng M, Xian D, Pumin H, Huiliang L. Preparation research of novel composite phase change materials based on sodium acetate trihydrate. *Appl Therm Eng* 2017; 118:817–25. <https://doi.org/10.1016/j.applthermaleng.2017.02.102>.
- [42] Dannemad M, Johansen JB, Furbo S. Solidification behavior and thermal conductivity of bulk sodium acetate trihydrate composites with thickening agents and graphite. *Sol Energy Mater Sol Cells Int J Devoted Photovolt Phototherm Photochem Sol Energy Convers* 2016;145:287–95. <https://doi.org/10.1016/j.solmat.2015.10.038>.
- [43] Cui W, Yuan Y, Sun L, Cao X, Yang X. Experimental studies on the supercooling and melting/freezing characteristics of nano-copper/sodium acetate trihydrate composite phase change materials. *Renew Energy* 2016;99:1029–37. <https://doi.org/10.1016/j.renene.2016.08.001>.
- [44] Mohamed Moussa EI, Karkri M. A numerical investigation of the effects of metal foam characteristics and heating/cooling conditions on the phase change kinetic of phase change materials embedded in metal foam. *J Energy Storage* 2019;26: 100985. <https://doi.org/10.1016/j.est.2019.100985>.
- [45] Velraj R, Seeniraj RV, Hafner B, Faber C, Schwarzer K. Heat transfer enhancement in a latent heat storage system. *Sol Energy* 1999;65:171–80. [https://doi.org/10.1016/S0038-092X\(98\)00128-5](https://doi.org/10.1016/S0038-092X(98)00128-5).
- [46] TESS-Thermal Energy Systems Specialists. TESSLibs 17 HVAC Library Mathematical Reference. TESSLibs 2012;17(06):1–262.
- [47] Yazaki Corporation Company. Water Fired Absorption Chillers 2017:15. <https://www.yazakienergy.com/>.
- [48] Shirazi A, Taylor RA, Morrison GL, White SD. A comprehensive, multi-objective optimisation of solar-powered absorption chiller systems for air-conditioning applications. *Energy Convers Manag* 2017;132:281–306. <https://doi.org/10.1016/j.enconman.2016.11.039>.
- [49] Mehmood S, Maximov SA, Chalmers H, Friedrich D. Energetic, Economic and Environmental (3E) Assessment and Design of Solar-Powered HVAC Systems in Pakistan. *Energies* 2020;13:4333.
- [50] Sukkur Electric Power Company. Consumer Gas Prices n.d. <https://bill.pitc.com.pk/> (accessed August 10, 2022).
- [51] Yousuf I, Ghumman AR, Hashmi HN, Kamal MA. Carbon emissions from power sector in Pakistan and opportunities to mitigate those. *Renew Sustain Energy Rev* 2014;34:71–7. <https://doi.org/10.1016/j.rser.2014.03.003>.
- [52] Sui Northern Gas Pipelines Ltd. Consumer Gas Prices n.d. <https://www.sngpl.com.pk/> (accessed August 10, 2022).
- [53] Hmadi M, Mourtada A, Daou R. Forecasting the performance of a district solar thermal smart network in desert climate – A case study. *Energy Convers Manag* 2020;207:112521. <https://doi.org/10.1016/j.enconman.2020.112521>.

- [54] Baniyounes AM, Rasul MG, Khan MMK. Assessment of solar assisted air conditioning in Central Queensland's subtropical climate. *Australia Renew Energy* 2013;50:334–41. <https://doi.org/10.1016/j.renene.2012.06.042>.
- [55] Uçkan İ, Yousif AA. Investigation of the effect of various solar collector types on a solar absorption cooling system. *Energy Sources, Part A Recover Util Environ Eff* 2021;43:875–92. <https://doi.org/10.1080/15567036.2020.1766599>.
- [56] Nos M, List P, Spe V. Technical Data Manual VITOSOL 200 Type SP Vacuum tube collector based on the heat pipe principle For the utilisation of solar energy Vitosol 200. SP Technical Data 2016:1–12.